ACS NANO

www.acsnano.org

ARTICLE

Spatiotemporally Resolved Protein Detection in Live Cells Using Nanopore Biosensors

Hongshuai Zhang, Tao Zhao, Peifeng Huang, Qingsong Wang, Hao Tang,* Xia Chu, and Jianhui Jiang*

Cite This: *ACS Nano* 2022, 16, 5752–5763

Read Online

ACCESS | Metrics & More | Article Recommendations | Supporting Information

ABSTRACT: **Spatiotemporal detection of proteins in living cells is a persistent challenge but is the key to understanding their cellular biology and developing theranostic technologies. We develop a dual-nanopore biosensor using affinity-tunable peptide probes, which enables label-free and spatiotemporal monitoring of protein abundance and its concentration change in single live cells. We demonstrate that by screening for peptide probes with tunable affinities, the nanopore modified with a medium-affinity peptide allowed reversible and sensitive detection of the protein kinase A (PKA) catalytic subunit with a detection limit of 0.04 nM. The sensor is shown to have the ability to effectively eliminate interferences from cell membrane resistance and coexisting species in live cell detection. Moreover, our sensor is successfully implemented in monitoring of dynamic PKA activity changes (PKA catalytic subunit dynamic concentration changes) under different stimulations in single live cells. Our design may provide a paradigm for developing nanopore biosensors for spatiotemporally resolved protein analysis in live cells.**

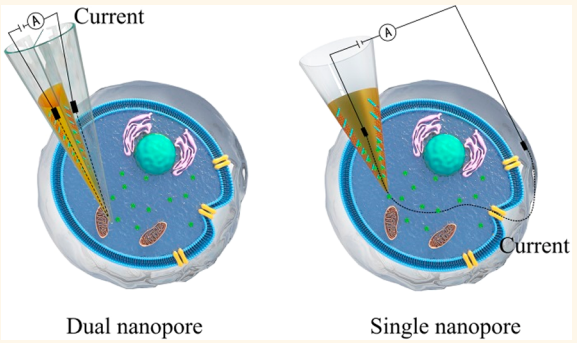

KEYWORDS: *spatiotemporally resolved detection, nanopore biosensors, reversible protein sensing, single-cell analysis, affinity-tunable peptides*

INTRODUCTION

Proteins are among the most important molecules that exert crucial functions in cellular systems. The expression and activity of proteins are dynamically and tightly regulated in various signaling pathways. Techniques that enable spatiotemporal resolution of protein dynamic concentration changes in single live cells are essential for cellular biology and biomedical applications. Despite the great success of various biosensors based on natural interaction partners[1,2] or artificially engineered antibodies,[3] aptamers,[4,5] and small-molecule ligands,[6] reversible biosensors that enable spatiotemporal monitoring of protein concentration changes in live cells have rarely been explored.

Nanopipette structures, which are characterized by nanopores opening at the tip, have provided a valuable tool for spatiotemporal resolution of molecular processes in single live cells.[7] The nanopipette structures show ionic transport properties depending on their characteristic parameters such as effective dimension and surface charge of the nanopores.[8−10] Specific modulation of these characteristic parameters provides a useful strategy to develop minimally invasive nanopore biosensors for spatiotemporally resolved interrogation of single cells.[11−13] The utility of nanopipette structures for sensor development can be performed either for single-molecule or bulk detection. Nanopore biosensors for single-molecule detection rely on real-time recording of transiently modulated ionic current due to the passage of single molecules through the nanopore.[14,15] The implementation of this type of nanopore sensor in live cells remains elusive because of their low signal-to-noise ratios and high working concentration.[16] The nanopore biosensors for bulk detection are based on ion current rectification (ICR), pore size changes, or redox currents induced by target-specific interactions or reactions.[17−22] These nanopore sensors have demonstrated a success in in vitro applications.[17−19] However, their implementation in live cells is still limited to a few targets such as glucose, H_2O_2, and NADH through redox reactions.[20−22] Nanopore sensors that enable spatiotemporally resolved detection of protein regulation dynamics in live cells remain a persistent challenge.

Received: December 6, 2021
Accepted: March 14, 2022
Published: March 17, 2022

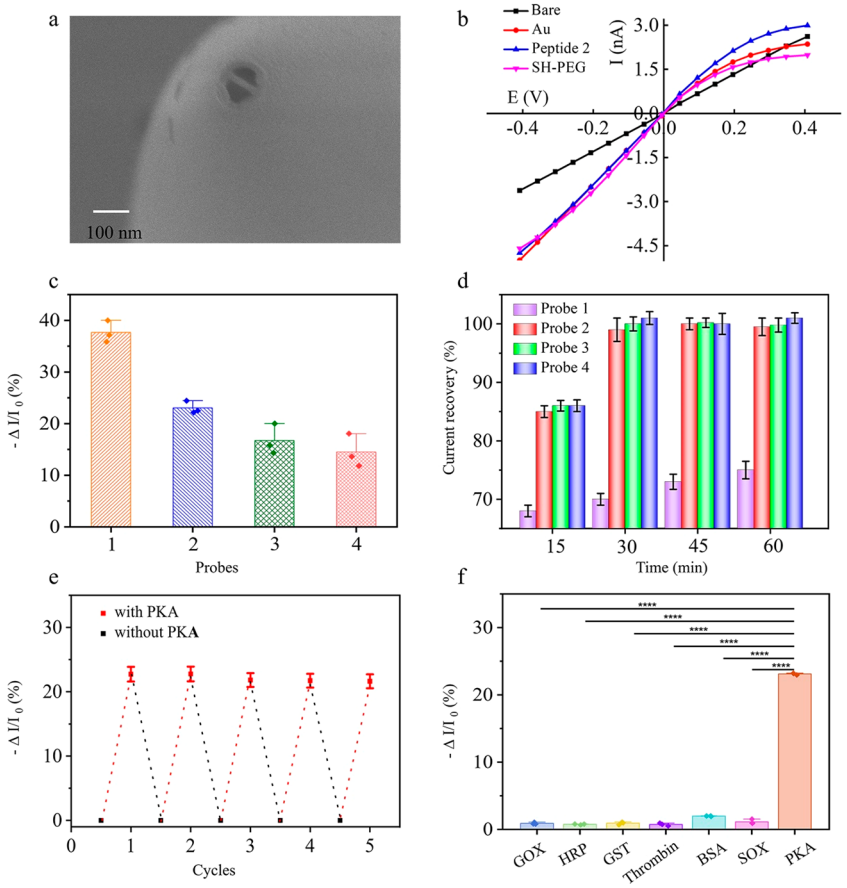

Figure 1. (a) SEM images of the dual nanopore. (b) $I-V$ curves of the dual nanopore with different modification on the inner surface. (c) Current responses to the 2.5 nM PKA catalytic subunit of the dual nanopore modified with peptide probes 1−4 (sequences shown in Table S1). (d) Current recovery of dual nanopore modified with peptides 1−4 and PEG after immersing in PBS for varying times. (e) Current responses ($-\Delta I/I_0$ at −0.4 V) to 2.50 nM PKA catalytic subunit of the dual nanopore modified with peptide 2 and PEG in regeneration assays through five cycles of immersion in PBS for 30 min, interaction with the PKA catalytic subunit solution for 15 min, and current measurements. (f) Current responses of the dual nanopore modified with peptide 2 and PEG toward the 2.5 nM PKA catalytic subunit and different proteins of 5 μM concentration. Statistical comparison was performed by a two-tailed t test, ****$P < 0.0001$. The error bars are standard deviations across three repetitive trials for plots c, d, and e.

We reason that the challenges of developing nanopore biosensors for spatiotemporally resolved living cells lies in the low and dynamically changed protein abundance in live cells and the current blockade due to the cell membrane in electric detection. To address the challenges, we propose a dual-nanopore biosensor through tethering affinity-tunable peptide probes on the inner surface of a dual-pore nanopipette, which enables reversible, label-free detection of protein in single live cells. First, the design of a reversible biosensor protein detection was proposed through elaborately tuning the affinity of inhibitor peptides toward target proteins. The reversibility is crucial for the utility of the biosensor to monitor temporal concentration changes of the target protein, as irreversible sensors cannot follow concentration decreases. Peptide probes can, in principle, be screened via various peptide display technologies toward any protein target.[23,24] Unlike antibodies for immunoassays, peptide probes confer tunable affinity to target proteins via facile sequence variations, allowing reversible, sensitive, and temporally resolved protein detection. The concept of tunable affinity for temporally resolved reversible biosensors can be extended to other biological recognition ligands such as antibodies or aptamers, provided that these ligands with tunable affinities are available. Second, the reversible nanopore biosensor is explored for temporally resolved protein kinase A (PKA) detection or monitoring its temporal concentration changes in single live cells. To our knowledge, nanoscale biosensors have not been explored for live cell detection of proteins, in particular, their time-dependent dynamics in concentration changes. Third, a dual-nanopore architecture is introduced in place of the commonly used single nanopore for single live cell detection. The dual-pore architecture works through an intrapipette electric circuit instead of the cross-membrane circuit for the single-pore architecture, which allows eliminating the current blockade from the cell membrane. Compared to the two single-nanopore pipettes design, this dual-pore architecture minimizes the difficulty in high-precision operation and the complexity of micromanipulation systems.

We demonstrated our dual-nanopore biosensor using PKA, the key molecule responsible for all cellular processes due to the cAMP second messenger system with crucial functions in many fundamental cellular processes such as energy metabolism, muscle contraction, membrane transport, and gene expression.[25] The PKA holoenzyme, which comprises two regulatory and two catalytic subunits, has no kinase activity. Binding of cAMP to the regulatory subunit unleashes the catalytic subunit with full PKA activities to phosphorylate their targets. We explored utilizing peptide probes specifically

https://doi.org/10.1021/acsnano.1c10796
ACS Nano 2022, 16, 5752−5763

recognizing the PKA catalytic subunit with varied affinities.[26] We envisioned that the tunable affinities allowed identification of a peptide probe for efficient but reversible capture of the PKA catalytic subunit on the inner nanopore surface. The capture of catalytic subunit on the inner surface can induce steric hindrance and charge change in the nanopore, modulating the ionic current signal and allowing detection of the PKA activity (or concentration of PKA catalytic subunit). The nanopore sensor allows reversible and sensitive detection of the PKA catalytic subunit with a detection limit of 0.04 nM, which is typically lower than the intracellular PKA activities in common cell lines and suggests its potential for live cell detection.[27,28] This reversible target-mediated current response may make the dual-nanopore sensor a promising platform for spatiotemporal resolution of protein dynamic concentration changes in single cells.

RESULTS AND DISCUSSION

Construction and Characterization of a Dual-Nanopore Biosensor. The dual-nanopore biosensor was fabricated using a dual barrel of the quartz capillary by laser pulling to obtain a nanopipette structure with two adjacent pores.[29] The diameters of two pores were ~50 nm, as characterized by scanning electron microscopy (SEM) (Figure 1a). The dual-nanopore architecture was further validated by fluorescence microscopic images of different fluorescent dye solutions separately added into the two barrels (Figure S1). The ion current rectification (ICR) effect is a phenomenon in which the asymmetric potential-dependent ion fluxes through an asymmetric, surface-charged conical nanopore when the pore diameter is on the order of the Debye screening length.[30] Ascribed to the symmetric nanopore architecture with similar surface charge,[31] the bare dual-pore nanopipette showed typical ohmic response with no negligible ICR effect (Figure 1b). The ohmic responses were also observed with different nanopore diameters and electrolyte concentrations (Figure S2).

The dual-nanopore architecture was characterized utilizing finite-element analysis.[30,32] The simulation revealed an asymmetric electric field distribution in two nanopores and the major potential drop at the tip directly connecting with the negative electrode with little potential drop at the other tip (Figure S3). A further numerical simulation for potassium ion flow direction revealed that potassium ions flowed from the nanopore connecting with the positive electrode to the other nanopore, and the ion flow exhibited a near-surface behavior (Figure S4). The enhancement of electric field and ion concentration at the tip of the dual nanopore was in agreement with previous simulation results of the single nanopore.[30] The current−voltage curves were also simulated for different KCl concentrations. An ohmic current response with no distinct ICR effect was observed (Figure S5), which were consistent with the above experiment results.

The bare dual-nanopore nanopipette was used to construct the biosensor through a three-step treatment, coating of gold film on the inner surface of one of the dual nanopores, self-assembly of peptide probes via their terminal cysteine moieties and blocking with mPEG-thiol 2000 to minimize nonspecific adsorption (Figure S6). The gold film deposition on the inner nanopore surface was verified by energy-dispersive spectroscopy data of the tip, tip appearance photograph, and absorption spectrum of the $HAuCl_4$ solution before and after the deposition (Figures S7−S9). The gold film deposition on one nanopore surface resulted in a distinct ICR response in KCl electrolyte solution because the chloride ion could form a chemisorption bond with the gold surface to increase its negative surface charge compared to that with a bare glass surface (Figure 1b).[33] ICR signals were also observed after subsequent self-assembly of peptide probes and thiolated PEGs on the gold film. (Note: Assembly using a peptide concentration <10 μM gave compromised sensitivity in PKA detection, probably due to the low coverage of the peptide on the pore surface.) The varied ICR signals were attributed to the changes of inner surface properties arising from the corresponding modifications. The density of peptides was estimated to be ~1.29 peptides/nm^2 using a FAM-labeled peptide for self-assembly on the gold-coated single-pore barrel followed by displacement with dithiothreitol.[34]

In Vitro Reversible PKA Activity Detection by the Peptide-Modified Dual-Nanopore Biosensor. The dual-nanopore biosensor with peptide probes was investigated for its responsive characteristics to the PKA catalytic subunit. With peptide probes with slight sequence variations, we obtained probes **1**−**4** with increasing dissociation constants ranging from 2.3 nM to 4.2 μM for the PKA catalytic subunit.[26] We found that the biosensors modified with these peptide probes showed decreased ionic current in response to the 2.5 nM (1.0 U/mL) PKA catalytic subunit, and the decrements of current responses increased with increasing affinities of peptide probes (Figure 1c and Figure S10). This finding suggested improved sensitivity arising from a peptide probe of higher affinity. A regeneration assay showed that the biosensors with peptide probes **2**, **3**, and **4** with lower affinities exhibited better reversibility, and immersion of the nanopipette in a phosphate-buffered saline (PBS) within 30 min allowed 99% current recovery (I/I_0 at −0.4 V) for the biosensor (Figure 1d). A further reusability assay revealed that the biosensor modified with peptide **2** could be used more than five times without loss of sensitivity through regeneration in PBS for 30 min (Figure 1e). This finding confirmed our hypothesis that peptide probes of tunable affinities enabled development of nanopore biosensors for reversible detection of the PKA catalytic subunit. We chose the biosensor constructed using peptide probe **2** with medium affinity in further experiments because it had excellent reversibility and higher sensitivity due to the improved affinity.

The biosensor constructed with peptide probe **2** displayed distinct (23.0 ± 0.5% current decrease) and specific response to the 2.5 nM PKA catalytic subunit, and little current signal changes were observed in control experiments using the constructed biosensor for detecting other proteins (Figure 1f). Recalling that the PKA holoenzyme in its multimeric form comprised two regulatory and two catalytic subunits and had no kinase activity, we tested the nanopore sensor with the PKA holoenzyme to examine whether peptide probe **2** might artificially dissociate the PKA holoenzyme to release catalytic subunits. Only negligible current change was observed with the 1.2 nM PKA holoenzyme utilizing a nanopore sensor modified with peptide **2** and PEG, whereas a distinct current change appeared after 15 min with addition of excess cAMP (100 nM) (Figure S11). The result suggested that the nanopore had no response to the PKA holoenzyme or would not dissociate the PKA holoenzyme to release catalytic subunits, and the current decrease signals were specific to the binding of the catalytic subunit or the cAMP-released catalytic subunit from the holoenzyme. A further control assay using a gold-coated

https://doi.org/10.1021/acsnano.1c10796
ACS Nano 2022, 16, 5752−5763

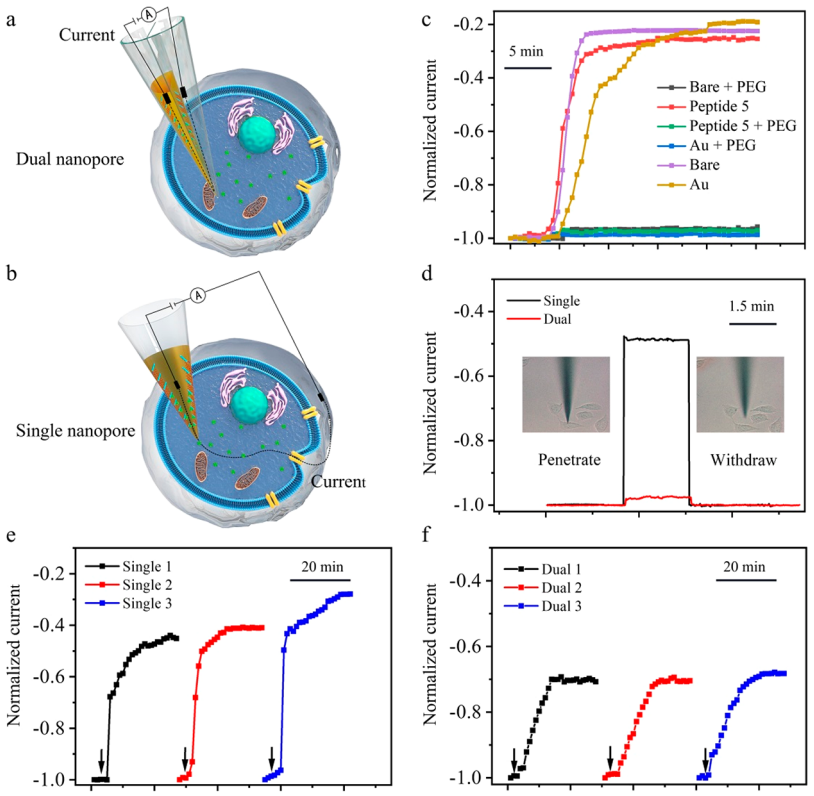

Figure 2. (a,b) Architecture of dual-nanopore versus single-nanopore biosensor in single-cell detection. (c) Time-dependent current recording of different dual nanopore surfaces in cell penetration. (d) Time-dependent current responses of single-nanopore and dual-nanopore biosensor through cell penetration to retraction. (e) Time-dependent current responses in single-cell detection of the PKA catalytic subunit with three individual single-nanopore biosensors. (f) Time-dependent current responses in single-cell detection of the PKA catalytic subunit with individual dual-nanopore biosensors in three representative assays. Current responses on the *y*-axis were correlated to PKA catalytic subunit concentration. The black arrow indicates penetration of the single cell by a nanopore. All time-dependent current responses are normalized to a baseline value of 1.0 by dividing a constant.

nanopore modified with thiolated PEG displayed only negligible current change in detection of PKA catalytic subunit (Figure S12), indicating that the response of the constructed biosensor to the PKA catalytic subunit was attributed to the specific interaction between peptide **2** and the PKA catalytic subunit. Another control experiment using a gold-coated nanopore modified with a nonbinding peptide **5** with or without PEG blocking for cell lysate detection showed that the PEG-blocked biosensor had negligible responses, whereas the biosensor without PEG blocking gave a substantial current decrease (Figure S13). This result suggested that the PEG blocking was essential for precluding nonspecific adsorption from interferents in the complex biological matrix. Moreover, we still obtained a substantial current decrease (17% current decrease) in closer interrogation of the constructed biosensor for detecting the PKA catalytic subunit in 1 M KCl (Figure S14), a high electrolyte concentration that minimized the effect of surface charge of the nanopore on the current signal.[17] The high-concentration electrolyte solution experiment showed that the surface charge changes only contributed to minor ion current changes, suggesting the change of effective pore size was the major mechanism of our nanopore sensor.

Additional experiments showed that the current response decreased slightly with increase size of the nanopores (Figure S15), seemingly attributed to the decreased contribution of protein binding to the pore size reduction. Our preceding simulations (Figures S3–S5) showed that ion flow was not evenly distributed in the nanopore with higher ion concentration in the electrical double layer near the inner surface. Thus, the major current was contributed by the ions transporting near the inner surface. As the confined ionic responses became decreased with increasing nanopore diameter,[31] we reasoned that they mainly originated from the pore opening or along the whole inner surface at the nanoscale tip. In our PKA sensor, we expected major ionic responses at the nanopore opening, as the mass transfer and the accompanied inner surface–protein interaction were facilitated at the pore opening. On the other hand, because capture of proteins also took place on the nanopore inner surface, dramatic steric hindrance to ion transport would be generated by protein binding near the inner surface, inducing substantial decrease in the ion current. This reasoning suggested a dependence of ion current responses upon the protein size and the protein configuration on the inner surface. To validate it, we performed a further experiment using a streptavidin (SA)-conjugated PKA catalytic unit via biotin–SA interactions and found that the larger SA-conjugated protein induced higher current response (Figure S16). This result clearly evidenced the dependence of current signals upon protein size or configuration. Furthermore, direct evidence for the binding of the PKA catalytic subunit via peptide probe recognition was obtained using the FITC-labeled PKA catalytic subunit in the assay, as strong fluorescence was observed in the tip of the nanopore (Figure S17).

The dual-nanopore biosensor modified with peptide **2** and PEG demonstrated high sensitivity and rapid kinetics for PKA

https://doi.org/10.1021/acsnano.1c10796
ACS Nano 2022, 16, 5752–5763

catalytic subunit detection. The current decreases were dynamically correlated to the PKA catalytic subunit concentrations in the range of 0.12 to 25 nM (Figure S18A,B). A linear correlation was achieved from 0.12 to 3.75 nM with an estimated limit of detection (LOD) of 0.04 nM (Figure S18C). The LOD value was typically lower than the intracellular PKA activities in common cell lines,[27,28] indicating the potential of the biosensor for live cell detection. Taking the average size of 17.1 μm for HeLa cells as a rough estimate,[35] we calculated that the volume of a single cell was ~3 pL. The LOD of 0.04 nM amounted to ~72 PKA catalytic subunits per cell, and the dynamic range of 0.12 to 25 nM amounted to ~215 to 45000 PKA catalytic subunits per cell, indicating the capability of our nanopore sensor for detecting the binding of thousands of proteins inside the cells. To further investigate the selectivity, we tested the responses of the varying concentrations of the PKA catalytic subunit in undiluted serum. A consistent result was obtained, indicating that the nanopore sensor could preclude nonspecific interactions from interferents in complex biological matrices (Figure S19).

Time-dependent recording of the current signals in a titration assay of three consecutive additions of the PKA catalytic subunit revealed a response of the biosensor within <13 min (Figure S20). The time scale was similar to that for PKA activity changes in live cells,[36] implying the potential of the nanopore biosensor for real-time monitoring of PKA dynamic concentration changes in cells. To investigate the stability of the biosensor, we performed extensive characterization of the stability of the $I-V$ (current versus potential) signals and $I-t$ (current versus time) signals over 30 min (Figures S21 and S22). The results revealed that both $I-V$ and $I-t$ signals were stable over the period. According to Langmuir adsorption and Scatchard plot analysis,[37] we estimated the dissociation constant for the immobilized peptide toward the PKA catalytic subunit to be ~27 nM (Figure S23). This value was in good approximation to the reported value (36 nM) for peptide **2** toward the PKA catalytic subunit.[26] The sensing principle was also applied to the single-nanopore architecture. Single-pore biosensors were also constructed via gold film coating followed by the peptide and PEG assembly. We found that the single-pore biosensors demonstrated in vitro analytical performances similar to those of the dual-nanopore design (Figures S24–26).

PKA Activity Detection in Single Living Cell with a Dual-Nanopore Biosensor. The dual-nanopore biosensor was utilized for PKA activity (catalytic subunit concentration) in single live cells using a homemade micromanipulation system (Figure 2a,b). We performed two separate tests to compare the performance of PEG blocking. Each test, either with PEG blocking or without PEG blocking, included three kinds of nanopore surfaces: (1) bare glass surface, (2) gold film coating, (3) modification with nonbinding peptide **5** on the coated gold film. The result showed that three kinds of nanopore surfaces with PEG blocking displayed little current changes upon penetrating into a cell (Figure 2c), demonstrating the critical role of PEG blocking in precluding nonspecific adsorption for the nanopore sensor in live cell detection. We then investigated the influence of current blockade from the cell membrane using the single-nanopore and the dual-nanopore configuration. Interestingly, the single-nanopore nanopipette modified with nonbinding peptide **5** and PEG blocking showed a large, abrupt current change upon penetrating into the cell and a reverse current change upon retraction (Figure 2d). By contrast, the proposed dual-nanopore configuration with nonbinding peptide **5** and PEG blocking demonstrated only slight current change through the penetration to retraction. We ascribed the abrupt current changes of the single-nanopore nanopipette to the cell membrane resistance involved in the current circuit. It was clear that the dual-nanopore design only involved an intrapipette electric circuit with the cell membrane resistance excluded from the circuit. Hence, the dual-nanopore configuration afforded an obvious advantage over the single nanopore in minimizing the effect of cell membrane resistance.

We then investigated the response of the developed nanopore biosensor modified with peptide **2** and PEG for PKA activity detection in living HeLa cells. When a cell was probed with the single-nanopore biosensor modified with peptide **2** and PEG, a sudden current change was observed upon penetration, followed by gradual current changes until saturation (Figure 2e). In parallel assays for three single cells, the single-pore sensor showed substantial deviations in the total current response amplitudes. We ascribed the large current response variability to the variations of cell membrane resistance across different cells. In contrast, no abrupt current changes appeared during penetration of the cells using the dual-nanopore biosensor modified with peptide **2** and PEG, and a gradual current change profile was obtained in the assay (Figure 2f). Moreover, the total current response amplitudes only exhibited slight discrepancy in assays for three single cells. This result demonstrated that the dual-nanopore architecture allowed mitigating the effect of cell membrane, implying the potential of the dual-nanopore biosensor for PKA activity detection in living cells. Therefore, we only used the dual-pore biosensor modified with peptide **2** and PEG for PKA activity detection in subsequent live cell studies. The intrinsic characteristic of the nanopipette sensor allowed it to be manipulated at a nanoscale precision to probe different sites in a live cell for real-time monitoring. Hence, we utilized the dual-pore biosensor to detect PKA activity at different sites along a z dimension in the cytoplasm of a live cell. The result shows that there are little variations in PKA activities at different sites in the cytoplasm (Figure S27), indicating the PKA catalytic subunits were evenly distributed in the cytoplasm. The biocompatibility of the nanopore sensor was further interrogated using propidium iodide (PI), a fluorescence dye only permeable to damaged cells but not to intact cells.[21] We found that negligible fluorescence was observed after insertion of the nanopore sensor (modified with peptide **2** and PEG) for 3 h in the cells and even after penetration in and retraction from the cells five times (Figure S28). This finding suggested that application of the nanopore sensor for live cell detection had little damage to the cells, which was consistent with previous observations that nanopipette structures had minimal cellular damage.[20−22] Even though the nonmodified outer surface of the quartz nanopipettes might have nonspecific adsorption of cellular components via hydrogen bonds or electrostatic interactions, we anticipated that the very tiny, negatively charged, and hydrophilic outer surface of the nanopipettes would only have minimum interference with the cells. Hence, we did not investigate the treatment of the outer surface of the nanopipettes, which was routinely used in current nanopipette-based live cell studies.[20−22] In addition, free diffusion of molecules between the nanopore sensor and the penetrated cell was validated using a fluorescent dye Cy3 (Figure S29).

https://doi.org/10.1021/acsnano.1c10796
ACS Nano 2022, 16, 5752−5763

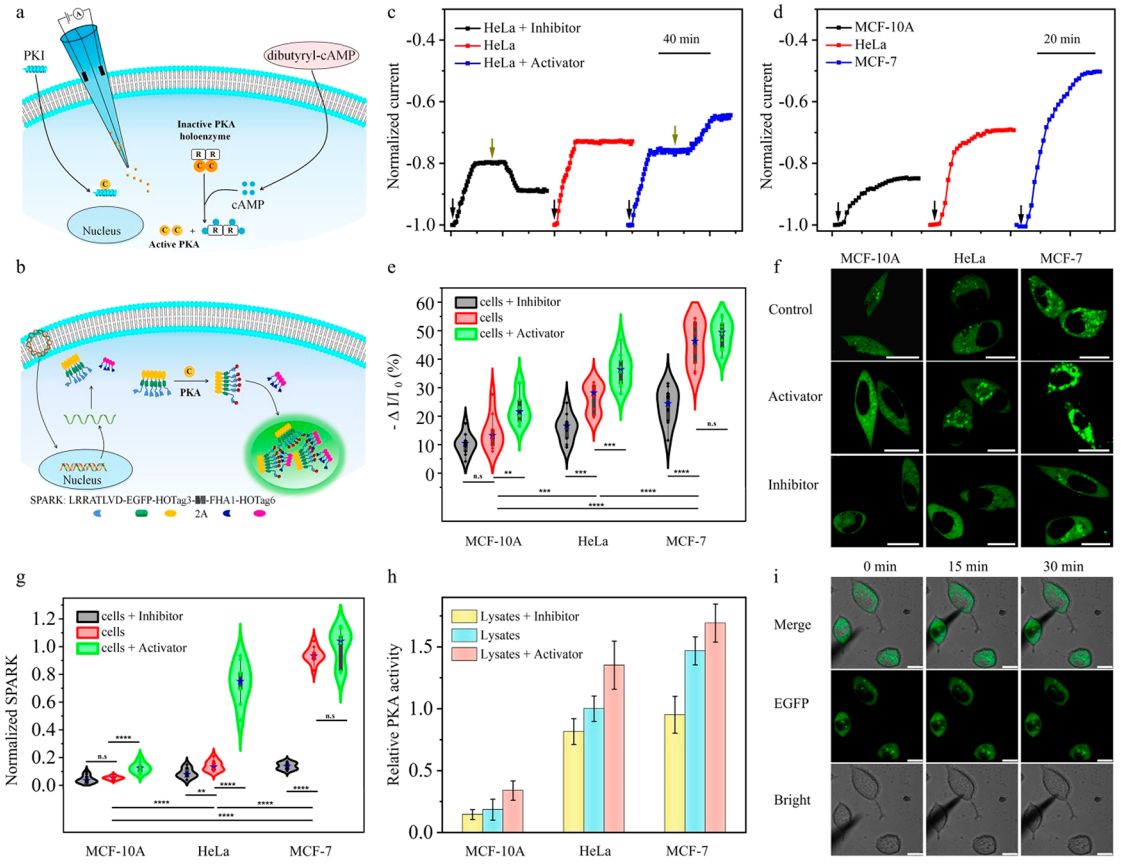

Figure 3. Schematic illustration of (a) dual-nanopore biosensor and (b) SPARK biosensor for single live cell PKA activity detection. (c) Time-dependent current recording in HeLa cells under PKA activator or inhibitor stimulations. (d) Time-dependent current response to PKA activity in three cell lines of MCF-10A, HeLa, and MCF-7. (e) Saturated current responses in three cell lines under activator or inhibitor stimulations. (f) Fluorescent imaging of PKA activity and (g) normalized SPARK signals with SPARK biosensor of three cell lines of MCF-10A, HeLa, and MCF-7 under PKA activator or inhibitor stimulations. The average SPARK signals from the response of activator-treated MCF-7 was normalized to 1.0. (h) PKA activities in three cell lines treated under activator or inhibitor stimulations determined using a commercial PKA assay kit. (i) Time-dependent SPARK images for a cell with a nanopore sensor inserted. The black arrow indicates penetration of the single cell by nanopore and the green arrow represents the addition of stimuli in c and d. Each violin plot in e and g represents measurements from 10 individual cells, and the pentacle indicates average value. (c,d,f,i) Representative data from three independent experiments. Scale bar: 10 μm. The error bars are standard deviations across three repetitive assays for h. Statistical comparison was performed by two-tailed *t* test; n.s. is not significant, *$P < 0.05$, **$P < 0.01$, ***$P < 0.001$, ****$P < 0.0001$. All time-dependent current responses are normalized to a baseline value of 1.0 by dividing a constant.

Real-Time Monitoring of PKA Dynamic Concentration Changes in Single Living Cell with Dual-Nanopore Biosensor. Since PKA activity was dynamically regulated in various cellular signaling pathways, the ability of the nanopore biosensor for detection of the dynamic PKA activity variations under different stimulations was investigated by real-time recording of the current responses during its insertion in a live cell (Figure 3a). We also used a genetically encoded fluorescent PKA activity biosensor, called SPARK (separation of phase-based activity reporter of kinase),[36] to cross-check our measurements of PKA activity. The principle of SPARK was based on two designer homo-oligomeric peptides. One peptide encodes the PKA peptide substrate (LRRATLVD) with a fluorescence protein EGFP and a homohexameric coiled coil (HOTag3), and the other encodes the phosphopeptide binding domain (FHA1) with a homotetramer coiled coil (HOTag6). Upon PKA activation, the PKA peptide substrate is phosphorylated followed by interaction with the FHA1 domain, which mediates cross-linking of two designer homo-oligomeric peptides and highly concentrated EGFP foci as the indicator for PKA activity (Figure 3b). We observed that upon penetration in a HeLa cell utilizing a nanopore sensor modified with peptide **2** and PEG, a gradual current change appeared until it became saturated with a 27% current decrease after ~15 min, corresponding to a 3.02 nM PKA catalytic subunit estimated from the calibration curve in Figure S18 (Figure 3c). To determine if the current changes were specific to PKA activity, HeLa cells were incubated with a high dose of a cell-permeable peptide inhibitor of the PKA catalytic subunit.[38] It could bind PKA catalytic subunits with higher affinity (2.3 nM) and block the binding of the catalytic subunits to the nanopore, decreasing the effective concentration of the PKA catalytic subunit inside the cells. As anticipated, much smaller current response amplitude (12% current decrease, corresponding to 1.25 nM PKA catalytic subunit) was obtained for the nanopore sensor modified with peptide **2** and PEG inserted in the inhibitor-treated cell (Figure S30). Moreover, the cell was treated with a PKA activator, dibutyryl-cAMP,[39] which was a cell-permeable analogue of cAMP to dissociate the PKA holoenzyme and increase the concentration of the PKA catalytic subunit inside the cells. An increased amplitude (41% current decrease, corresponding to 6.24 nM PKA catalytic

https://doi.org/10.1021/acsnano.1c10796
ACS Nano 2022, 16, 5752−5763

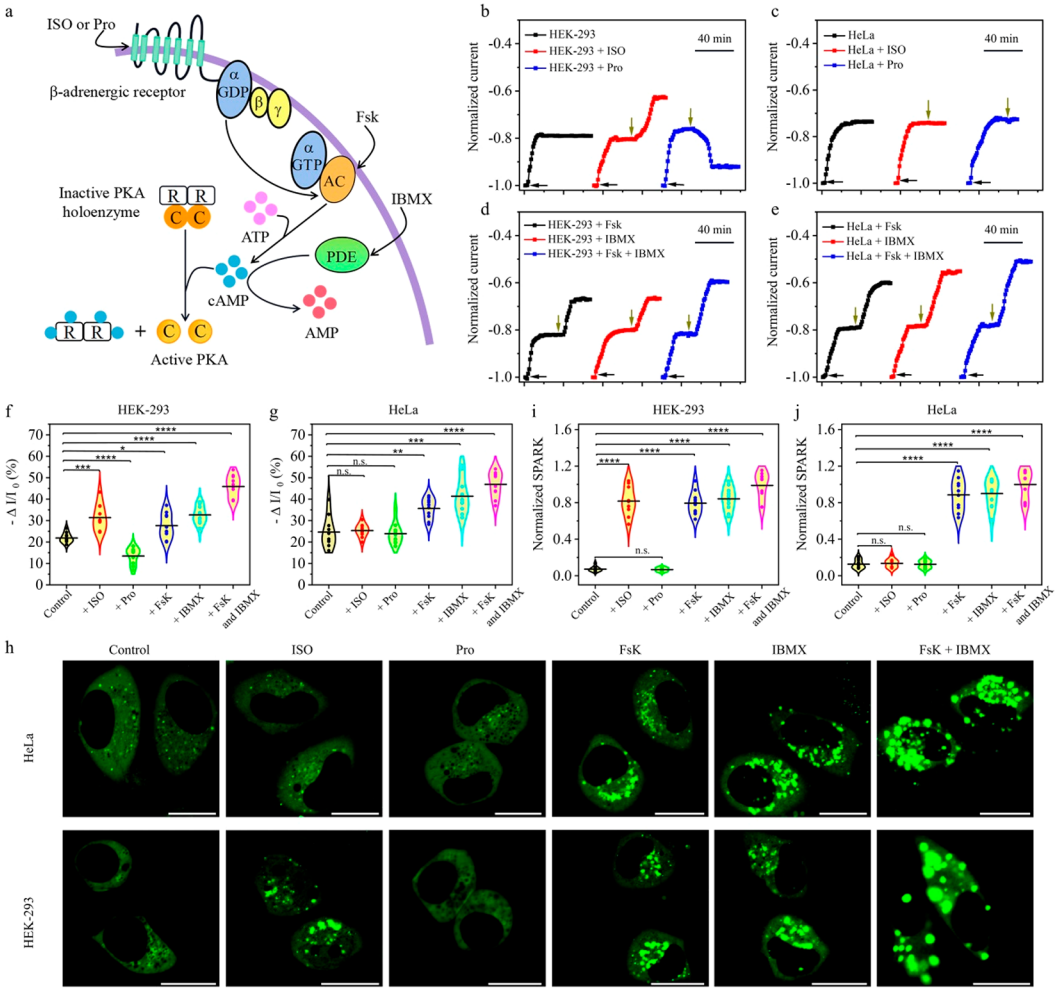

Figure 4. (a) Schematic illustration of signaling pathways from GPCR ligands to PKA activation. (b) Time-dependent current responses to dynamic PKA activity changes in HEK-293 cells with ISO or Pro stimulation. (c) Time-dependent current responses to dynamic PKA activity changes in HeLa cells with ISO or Pro stimulation. (d) Time-dependent current responses to dynamic PKA activity changes in HEK-293 cells induced by Fsk, IBMX, or FsK + IBMX. (e) Time-dependent current responses to dynamic PKA activity changes in HeLa cells induced by Fsk, IBMX, or FsK + IBMX. (f,g) Current responses to PKA activity in single HEK-293 or HeLa cell after 1 h stimulation of ISO, Pro, Fsk, IBMX, or Fsk + IBMX. (h) Fluorescence images of SPARK biosensor in HeLa and HEK-293 cell lines under 30 min different stimuli for detection of dynamic PKA activity changes. (i,j) Fluorescence responses to PKA activity in single HEK-293 or HeLa cells after 30 min stimulation of ISO, Pro, Fsk, IBMX, or Fsk + IBMX; the fluorescent intensity was normalized to 1.0 for the average signals from the response of Fsk + IBMX stimulation for the HeLa cell line. The black arrow indicates penetration of the single cell by nanopore and the green arrow represents the addition of stimuli in b−e. Each violin plot in panels f, g, i, and j represents measurements from 10 individual cells, with the crossing line indicating the average value. Statistical comparison was performed by two-tailed *t* test; n.s. is not significant, *P < 0.05, **P < 0.01, ***P < 0.001, ****P < 0.0001. (b−e,h) Representative data from three independent experiments. Scale bar: 10 μm. All time-dependent current responses are normalized to a baseline value of 1.0 by dividing a constant.

subunit) has been observed in the current response profile. This result confirmed the PKA-specific responses for the nanopore sensor modified with peptide **2** and PEG. A closer assay was performed for a single HeLa cell with further additions of the PKA activator or inhibitor after the nanopore or SPARK sensor was equilibrated in the cells (Figure 3c,f). We found that addition of the PKA activator triggered further current decrease down to another saturation, which was consistent with the enhancement of fluorescent foci obtained using the SPARK sensor. The addition of the PKA inhibitor induced partial recovery of the current signal of the nanopore sensor (modified with peptide **2** and PEG) and a consistent decrease of fluorescent foci from SPARK. This finding indicated that the biosensor was capable of specific and reversible monitoring of PKA dynamic concentration changes in single cells.

It is worth mentioning that, when no stimulations were applied, HeLa cells still showed obvious current responses for the nanopore sensor (modified with peptide **2** and PEG) and fluorescence foci for SPARK. This result verified a substantial basal level for PKA activity and the high sensitivity of the nanopore sensor. According to the working curve, we could estimate the average PKA activities in single cells to be 2.98 nM in HeLa cells, amounting to ∼5400 PKA catalytic subunits per cell based on an estimation of ∼3 pL volume of a single cell. The nanopore biosensor and SPARK were further used for basal PKA activity detection in different cell lines, MCF-10A, HeLa, and MCF-7. We observed that the nanopore biosensor (modified with peptide **2** and PEG) displayed varied current

https://doi.org/10.1021/acsnano.1c10796
ACS Nano 2022, 16, 5752−5763

change amplitudes in different cells (Figure 3d). The MCF-7 cells gave the highest current response, whereas the MCF-10A cell exhibited the lowest current change. Likewise, we estimated the average PKA activities in single MCF-10A and MCF-7 cells to be 1.60 and 5.20 nM, respectively. This result indicated an increasing basal PKA activity in MCF-10A, HeLa, and MCF-7 cells, which was consistent with the results obtained using SPARK (Figure 3f) and previously reported PKA activity in these cells.[27] The nanopore sensor modified with peptide **2** and PEG was further used for quantifying PKA activity in single live cells of different cell lines under treatments with inhibitors or activators (Figure 3e). We found that different cells (cell number 10) from the same cell line (a cell group) exhibited heterogeneous PKA activity. We ascribed the heterogeneous PKA activity in the same cell line to the single-cell heterogeneity, as the intragroup variations were substantially larger than the errors for repetitive assays of a cell lysate (Figure S31). The SPARK sensor also showed heterogeneous PKA activity among the same cell line (Figure 3f,g). The results showed consistent data that the PKA activities in MCF-7, HeLa, and MCF-10A cells were in decreasing order, and the cells treated with activators displayed higher activity, whereas the cells treated with inhibitors gave lower activity. Moreover, the current responses were in good agreement with relative PKA activities (normalized by PKA activity in HeLa cell lysate) in the corresponding cell lysates determined using a commercial colorimetric PKA assay kit (Figure 3h and Table S2). The cell lysate measurements from the commercial colorimetric PKA assay kit showed that the detected average basal PKA activities in single MCF-10A, HeLa, and MCF-7 cells are 1.00, 5.22, and 7.62 nM, respectively (Table S2). The values were acceptably approximate to those estimated using the nanopore responses, considering the complicated live cell surroundings. Together, these results demonstrated that the nanopore sensor modified with peptide **2** and PEG had the potential for detection of PKA activities in single living cells. A further control experiment revealed that negligible changes in the SPARK signals appeared after insertion of the nanopore sensor (modified with peptide **2** and PEG) in HeLa cells, suggesting that the penetration of our nanopore sensor had little effect on the basal PKA activity in the cells (Figure 3i and Figure S32).

We then asked whether the dual-nanopore biosensor had the ability to interrogate the dynamic concentration changes of the PKA catalytic subunit using two cell lines, HEK-293 cells with overexpressed β-adrenergic receptor (β-AR) and HeLa cells with low β-AR expression.[39] A typical PKA signaling pathway starts from β-AR activation, followed by GDP for GTP exchange in Gα of the heterotrimeric G proteins, adenylyl cyclase (AC) activation to convert ATP into cAMP and in turn PKA activation.[36,40] In addition to the main pathway, PKA activity was also down-regulated by phosphodiesterase (PDE) via hydrolysis of cAMP (Figure 4a). It is worth noting that since the PKA catalytic subunit was a product of the dissociation equilibrium between the PKA holoenzyme and cAMP, the catalytic subunit concentration was determined by PKA holoenzyme concentration and cAMP concentration. We did not distinguish the effects from concentration changes of cAMP or the PKA catalytic subunit but monitored the temporal concentration changes of the PKA catalytic subunit to understand the upstream pathways to regulating cAMP concentrations. First, we examined the regulation function of β-AR. After the nanopore sensor (modified with peptide **2** and PEG) penetrated HEK-293 cells, a rapid current decrease appeared and saturated within ~15 min, indicating an endogenous active PKA expression in the cells. Upon addition of the β-adrenergic agonist isoproterenol (ISO), we observed a further decrease of the current signal until stabilization within ~20 min (Figure 4b). In contrast, addition of the β-adrenergic antagonist propranolol (Pro) resulted in a gradually increased current signal until stabilized in ~20 min. Note that Pro did not completely blocked PKA activity, and there was partial residual activity, which could be ascribed to the insufficient dosage of Pro for complete inhibition of the upstream GPCR signaling or the presence of other pathways involved in PKA activation. On the other hand, the biosensor almost exhibited negligible response to ISO and Pro stimulations in β-AR-negative HeLa cells (Figure 4c). The results implied that the biosensor was capable of monitoring the dynamic PKA activity changes regulated by β-AR in β-AR-positive cells, PKA activity up-regulation under ISO stimulation, and PKA activity down-regulation under Pro induction, consistent with the literature data that used genetically encoded fluorescent biosensors for intracellular PKA activity detection.[36,39,40] Second, we investigated the regulatory roles of AC and PDE in the PKA signaling pathway. Upon stimulation with forskolin (Fsk) to activate AC and elevate cAMP, decreased current responses were observed as indicators for increased PKA activities in HEK-293 and HeLa cells. With the addition of 3-isobutyl-1-methylxanthine (IBMX) that inhibited PDE and increased cAMP concentrations, we also obtained elevated PKA activities in both cell lines. Even higher PKA activities were found for HEK-293 and HeLa cells incubated with Fsk and IBMX (Figure 4d,e). These results were in good agreement with previous reports,[36,39,40] suggesting that the biosensor had the ability to monitor dynamic PKA activity changes regulated by AC activation or PDE inhibition. Additionally, the nanopore biosensor was further used for detection of PKA activities in single HEK-293 and HeLa cells with 10 repeated trials after 1 h stimulation of ISO, Pro, Fsk, or IBMX (Figure 4f,g). Elevated PKA activities were obtained in HEK-293 cells after ISO, Fsk, and IBMX stimulation, and decreased PKA activities were achieved with Pro induction, with the highest PKA activity found with Fsk and IBMX co-stimulation. In HeLa cells, negligible changes of PKA activities were found upon ISO or Pro induction, but elevated PKA was observed after stimulation of Fsk or IBMX, and co-stimulation of Fsk and IBMX gave the highest PKA activity. These observations indicated that these stimulations could have a sustained effect on PKA activity for over 1 h. Together, the results revealed that the nanopore biosensor provided a promising platform for direct monitoring of PKA signaling and dynamic activity changes under different stimulations in single living cells. We also measured the dynamic PKA activity changes of HEK-293 and HeLa cell lines utilizing the SPARK sensor under these stimulations. We found that β-AR-negative HeLa cells displayed negligible PKA activity changes upon ISO and Pro stimulations, and β-AR-positive HEK-293 cells exhibited substantial activation and inhibition in response to ISO and Pro, respectively (Figure 4h,i,j), and the responses were both very rapid and completed within ~20 min (Figures S33 and S34). Moreover, HEK-293 and HeLa cells both showed increased PKA activity after ~15 min stimulation of Fsk or IBMX and further enhanced PKA activity upon co-treatment of Fsk and IBMX. This result was in good agreement with those obtained with the dual-nanopore biosensor, demonstrat-

https://doi.org/10.1021/acsnano.1c10796
ACS Nano 2022, 16, 5752−5763

ing that our nanopore biosensor was capable of monitoring the dynamic PKA activity change in live cells.

CONCLUSION

We reported a dual-nanopore biosensor for reversible, sensitive, and label-free detection of PKA in single living cells by engineering the nanopore inner surface with self-assembled affinity-tunable peptide probes. We showed that, by screening for peptide probes with tunable affinities, the nanopore sensor modified with a medium-affinity peptide probe enabled reversible and sensitive PKA activity detection. The sensor delivered current responses dynamically correlated to concentrations of the PKA catalytic subunit in the range of 0.12−25 nM with a detection limit of 0.04 nM. We also unraveled that the major current response of the sensor was ascribed to the decreased effective pore size due to protein binding. In vitro and live cell assays revealed that PEG blocking of the sensor surface allowed precluding nonspecific adsorption from interferents in the complex biological matrix. Moreover, the dual-pore architecture was shown to effectively eliminate the interference of cell membrane resistance in live cell current detection. Live cell assays revealed that the sensor had the capability of detecting PKA activities and direct monitoring of PKA signaling and dynamic activity changes in single living cells. The sensor exhibited excellent biocompatibility with little damage to the investigated living cells. Therefore, our nanopore sensor could provide a valuable paradigm for developing nanopore biosensors for spatiotemporally resolved protein analysis in living cells. We envisioned that an intelligent micromanipulation instrument, which integrated a microscope to real-time visualize the cells, a software to localize the cells and the nanopore probes, and a control motor system to automatic and accurate position the nanopore inside or outside the cells, could further expand the potential of the nanopore approach for large-scale or high-throughput assay in biomedical applications.

EXPERIMENTAL SECTION

Preparation of Single-Nanopore and Dual-Nanopore Nanopipettes. The quartz capillaries were thoroughly cleaned by sonicating in acetone, ethanol, and deionized water for 30 min each and dried prior to use. The dual-nanopore nanopipette was fabricated utilizing a P-2000 laser puller (Sutter Instrument, USA) from quartz theta capillaries (QF120-90-7.5, Sutter Instrument, USA). The inner diameter of the quartz theta capillary was 0.9 mm and divided into two barrels by a 0.15 mm thick septum. The dual-nanopore was fabricated by a laser-pulling process using a two-step process. Different parameters were utilized for fabrication of different pore diameters. For fabrication of a ∼30 nm nanopore, (1) Heat = 850, Fil = 4, Vel = 30, Del = 160, Pull = 80 followed by (2) Heat = 860, Fil = 3, Vel = 20, Del = 140, Pull = 160 was utilized. For fabrication of ∼50 nm nanopore, (1) Heat = 820, Fil = 4, Vel = 30, Del = 160, Pull = 80 followed by (2) Heat = 850, Fil = 3, Vel = 20, Del = 140, Pull = 160 was utilized. For fabrication of ∼70 nm nanopore, (1) Heat = 820, Fil = 4, Vel = 30, Del = 160, Pull = 80 followed by (2) Heat = 800, Fil = 3, Vel = 30, Del = 140, Pull = 160 was utilized. For fabrication of ∼100 nm nanopore, (1) Heat = 800, Fil = 4, Vel = 30, Del = 160, Pull = 80 followed by (2) Heat = 800, Fil = 3, Vel = 30, Del = 140, Pull = 160 was utilized. The single-nanopore nanopipette was fabricated using regular quartz capillaries with an inner diameter of 0.5 mm (QF100-50-7.5, Sutter Instrument, USA) using the following protocol: Heat = 860, Fil = 3, Vel = 30, Del = 140, Pull = 160.

Fabrication of Dual-Nanopore and Single-Nanopore Biosensors. To construct the dual-nanopore biosensor with a ∼50 nm pore, we utilized a quality control procedure to improve the reproducibility of the nanopore size. We measured the ionic current of the prepared nanopipettes (about −2.7 nA in 1× PBS under −0.4 V), and only the nanopipettes with current variations within 10% were chosen for biosensor construction. Then one nanopore surface was coated with a gold film, while the other nanopore surface was only modified with PEG. First, one barrel was injected with a 6 μL solution containing 1:4 (v/v) ethanol and 8 mM $HAuCl_4$ solution, and the other barrel was filled with distilled water. After illumination by UV light (254 nm, 18 W, model ZF-2, Anting Electronic Instrument Co. Ltd. Shanghai, China) for 2 h at room temperature, a thin gold film formed on the inner surface of one pore via photochemical reduction of chloroauric acid. The pore surface was washed with ethanol and distilled water and dried at 80 °C for 60 min. Then, a solution containing 10 μM peptide probes and 100 μM TCEP was injected into the gold-film-modified barrel and incubated for 12 h at room temperature to allow self-assembly of peptide probes on the inner surface via a Au−S bond. The unreacted reagents were removed by washing with 1× PBS thoroughly. Subsequently, 1 mM of SH-mPEG was injected to block the inner surface. The inner surface of the other pore was modified by incubating with 1 mM silane-mPEG at room temperature for 30 min. The single-nanopore biosensor was constructed using a similar procedure described above for the peptide-modified barrel.

Characterization of Dual-Nanopore and Single-Nanopore Architecture. Scanning electron microscopy was performed on a JSM-7800F instrument (JEOL, Japan) to characterize the structure of tip for the nanopore. Energy-dispersive spectroscopy was utilized to characterize the gold film coating on the inner pore surface. The success of gold film coating on the inner pore surface was also validated by measuring UV−vis spectra of $HAuCl_4$ solution before and after the reaction on a UV−vis spectrometer (UV 2450, Shimadzu, Japan). To determine the peptide density on a gold film surface, the gold-coated single-pore barrel modified with FAM-labeled peptide **2** was immersed in buffer solution (1.0 M dithiothreitol in 1× PBS, pH 8.0) for 12 h at room temperature. The solution was then collected for fluorescent measurement. The FAM-labeled peptide **2** samples for the standard curve were also prepared with the same buffer solution. The fluorescent measurements were performed with a FS5 spectrofluorometer with an excitation wavelength of 485 nm and emission collected at 522 nm. The bright-field and fluorescence images of the dual-nanopore architecture were obtained using a 20× objective lens on a confocal laser scanning fluorescence microscopy (Eclipse Ti and A1 confocal, Nikon, Japan). The 488 and 561 nm lasers were used as the excitation source for FITC and Cy3 solutions in two separate pores of the dual-nanopore nanopipette. The collection channels for FITC and Cy3 were in the range of 500−550 nm (green channel) and 575−625 nm (red channel), respectively. The 488 nm laser and FITC fluorescent channel of 500−550 nm was also utilized for validation of the interaction between FITC-labeled PKA and a peptide probe on the inner surface of the nanopore.

Numerical Simulation of a Dual Nanopore. The electric field distribution and ICR effect of the dual nanopore were investigated by finite-element analysis with commercial software COMSOL Multiphysics. A three-dimensional model was constructed to calculate the ionic current and electric field. Detailed information on the three-dimensional model is described in the Supporting Information Figures S35 and Table S3. The physical description was based on the Poisson−Nernst−Planck (PNP) equation.

$$\nabla^2\Phi = -\frac{F}{\varepsilon}\sum_i z_i c_i \tag{1}$$

$$J_i = -D_i\nabla c_i - \frac{z_i F}{RT}D_i c_i \nabla\Phi \tag{2}$$

The Poisson eq 1 describes the relationship between electric potential and ion concentration in the dual nanopore. The Nernst−Planck eq 2 describes the ion flux transportation in the dual nanopore. In these two equations, Φ is the electrical potential, z_i is the charge of species, c_i is the concentration, J_i is the ion flux, D_i is the diffusion

https://doi.org/10.1021/acsnano.1c10796
ACS Nano 2022, 16, 5752−5763

coefficient, and F, R, and T represent the Faraday constant, ideal gas constant, and the absolute temperature, respectively. The electroosmotic effect was ignored to simplify the simulation. The modeling was performed using steady-state conditions as depicted in eq 3.

$$\nabla \cdot J_i = 0 \tag{3}$$

The ionic current was obtained by integration of the ionic flux density passing through the dual nanopore as depicted in eq 4.

$$I = -F \int_S (J(K^+) - J(Cl^-)) \cdot n dS \tag{4}$$

The coupled eqs 1−4 could be solved with appropriate boundary conditions (Supporting Information Table S4).

In Vitro PKA Detection. A homemade electrochemical cell was utilized for current measurements of the nanopore biosensor, and two Ag/AgCl electrodes were used as the working electrode and reference electrode, respectively. For current measurement of dual-nanopore architecture, the two barrels were filled with electrolyte solutions of 1× PBS, 0.1 M KCl, or 1 M KCl, and two electrodes were separately placed into two barrels. For current measurement of a single-nanopore architecture, one electrode was placed in the barrel, while the other was placed in the solution bath. Electrochemical measurements of $I-V$ curves were performed by immersing the nanopore biosensor in the sample solution containing a specified concentration PKA. Effects of the $I-V$ measurements versus peptide probes with varying affinities, KCl concentrations, or tip sizes of the dual-nanopore nanopipette were also investigated. For control experiments, the constructed biosensor was used for detecting other proteins of GOX, HRP, GST, thrombin, BSA, and SOX with the same concentration of 5 μM and 2.5 nM PKA catalytic subunit. The gold-coated nanopore modified with 1 mM thiolated PEG was also used in a further control for detecting 2.5 nM PKA catalytic subunit. Regeneration of the nanopore biosensor was performed by immersing in 1× PBS for 30 min at room temperature.

Cell Culture and Single Living Cell Detection with a Dual-Nanopore Biosensor. HeLa cells, MCF-7 cells, or HEK-293 cells were cultured in fresh Dulbecco's modified Eagle's medium (DMEM) containing 10% fetal bovine serum (FBS), 50 U/mL penicillin, and 50 μg/mL streptomycin. MCF-10A cells were grown in fresh mammary epithelial cell growth medium (MEGM) containing BPE, rhEGF, insulin, hydrocortisone, GA-1000, and 100 ng/mL cholera toxin. Cells were cultured at 37 °C in a humidified atmosphere of 95% air and 5% CO_2 for 24 h, grown to 50−70%, and washed three times with 1× PBS (pH 7.4) solution before live cell measurements using the dual-nanopore biosensor.

Single living cell detection using the nanopore biosensor was performed as follows: First, the cell culture dish was placed on the microscope stage, and the single living cell was localized. Then the nanopore biosensor was mounted on the electrode holder and moved toward the single living cell using a three-dimensional micromanipulator. The micromanipulator had a ∼60 nm resolution for fine movement. The position of the nanopiptte at different sites along a z dimension can be controlled by the steps of the movement. Meanwhile, two electrodes were connected to a PGSTAT12 Autolab instrument for time-dependent current recording at a fixed interval of 1 s. We used a time scale method to allow the time-dependent current curves from different single-cell analysis to be clearly visualized. Also to compensate for variability among individual nanopores, we used a normalized ionic current by dividing the initial current measured in buffer solution before penetrating the live cell without changing the relative current decrease.[19] The initial current was normalized to −1.0 to indicate a negative ionic current. To investigate PKA signaling, HeLa cells, MCF-7 cells, or MCF-10A cells were treated under different stimulations, including a PKA activator (20 μL of 50 mM inhibitor into 1 mL of medium) or inhibitor (100 μL of 1.50 mM PKI into 300 μL of medium), AC activator (5 μL of 10 mM Fsk into 1 mL of medium), β-AR agonist (10 μL of 10 mM ISO into 1 mL of medium) or antagonist (10 μL of 10 mM Pro into 1 mL of medium), and PDE inhibitor (10 μL of 100 mM IBMX into 1 mL of medium).

For cell lysate extraction, 6−8 × 10^6 cells were collected and dispersed in 100 μL of RIPA lysis buffer (50 mM Tris, 150 mM NaCl, 1% Triton X-100, 1% sodium deoxycholate, 0.1% SDS, 1 mM sodium orthovanadate, 1 mM EDTA, and 1 mM PMSF, pH 7.4) followed by sonication for 15 s at 0 °C. The homogenates were centrifuged at 14000g for 50 min at 4 °C using a high-speed refrigerated centrifuge, and the supernatants were collected and stored at −80 °C before use. Then 30 μL of the cell lysates was utilized for PKA activities using a commercial PKA kit according to the instructions from the provider and calculated according to the calibration curve obtained with a set of standard PKA solutions.

Investigation on Cell Viability and Molecule Diffusion between Nanopipette and Cell. The effect of the nanopore sensor on cell viability was investigated by fluorescence imaging of the single HeLa cell incubated with PI. The single HeLa cell was penetrated using the nanopipette, following by keeping the nanopipette inside the cell for 180 min and retracting the nanopipette. After five times of this treatment, the cell was imaged for PI staining using a 532 nm laser as the excitation source and the emission of 550−620 nm. Molecule diffusion between the nanopipette and the cell was performed using a single MCF-7 cell penetrated by a nanopipette filled with Cy3 solution inside the barrel. Then diffusion of Cy3 in the cell was visualized through fluorescence imaging.

Living Cell PKA Imaging with SPARK. HeLa cells, MCF-10A cells, MCF-7 cells, and HEK-293 cells were transfected with the plasmid using Lipofectamine 3000. Cells were grown in 35 mm glass-bottom microwell (15 mm) dishes (NEST Corporation). Transfection was performed when cells were cultured to 30−60% confluence. For each transfection, 1.8 mg of plasmid DNA was mixed with 3.6 mg of Lipofectamine 3000, 0.1 mL of Opti-MEM medium, and 0.4 mL of DMEM. Cells were imaged 24 h after transfection using a 60× objective lens on a confocal laser scanning fluorescence microscopy (Eclipse Ti and A1 confocal, Nikon, Japan). The 488 nm laser and FITC fluorescent channel of 500−550 nm was utilized for fluorescence imaging. Time-lapse fluorescence images were acquired at 1 min interval with an exposure time of 60 ms. For stimulation experiments, the PKA activator (20 μL of 50 mM dibutyryl-cAMP into 1 mL of medium) or inhibitor (100 μL of 1.50 mM PKI into 300 μL of medium), AC activator (5 μL of 10 mM Fsk into 1 mL of medium), β-AR agonist (10 μL of 10 mM ISO into 1 mL of medium) or antagonist (10 μL of 10 mM Pro into 1 mL of medium), or PDE inhibitor (10 μL of 100 mM IBMX into 1 mL of medium) were added separately. Image acquisition was controlled by the NIS Elements Imaging Software (Nikon). For quantitative analysis of the fluorescence intensities, images were processed in ImageJ (NIH). The sum of the droplets' pixel fluorescence intensity and the cells' pixel intensity was scored using the Analyze Particle function in ImageJ, and the fluorescence intensities for each image were calculated as the sum of the droplets' pixel fluorescence intensity divided by cells' pixel intensity.

ASSOCIATED CONTENT

Supporting Information

The Supporting Information is available free of charge at https://pubs.acs.org/doi/10.1021/acsnano.1c10796.

Experimental details of materials, experimental setup, data acquisition, and sequences of different peptide probes; additional figures and tables for numerical simulation of dual-nanopore architecture and the characterization and validation of nanopore biosensors (PDF)

AUTHOR INFORMATION

Corresponding Authors

Hao Tang − *State Key Laboratory of Chemo/Biosensing and Chemometrics, College of Chemistry and Chemical Engineering, Hunan University, Changsha 410082, China;*

https://doi.org/10.1021/acsnano.1c10796
ACS Nano 2022, 16, 5752−5763

orcid.org/0000-0001-6392-5164; Email: haotang@hnu.edu.cn

Jianhui Jiang − *State Key Laboratory of Chemo/Biosensing and Chemometrics, College of Chemistry and Chemical Engineering, Hunan University, Changsha 410082, China;* orcid.org/0000-0003-1594-4023; Email: jianhuijiang@hnu.edu.cn

Authors

Hongshuai Zhang − *State Key Laboratory of Chemo/Biosensing and Chemometrics, College of Chemistry and Chemical Engineering, Hunan University, Changsha 410082, China*

Tao Zhao − *State Key Laboratory of Chemo/Biosensing and Chemometrics, College of Chemistry and Chemical Engineering, Hunan University, Changsha 410082, China*

Peifeng Huang − *State Key Laboratory of Advanced Design and Manufacturing for Vehicle Body, Hunan University, Changsha 410082, China*

Qingsong Wang − *State Key Laboratory of Fire Science, University of Science and Technology of China, Hefei 230026, China;* orcid.org/0000-0002-6686-195X

Xia Chu − *State Key Laboratory of Chemo/Biosensing and Chemometrics, College of Chemistry and Chemical Engineering, Hunan University, Changsha 410082, China;* orcid.org/0000-0002-4120-6131

Complete contact information is available at: https://pubs.acs.org/10.1021/acsnano.1c10796

Author Contributions

J.J. and H.T. conceived the project. H.Z., T.Z., H.T., X.C., and J.J. designed the experiments. H.Z. performed the experiments and data analysis with the help of T.Z. P.H. and Q.W. carried out the numerical simulations. The manuscript was written by H.T. and J.J. and edited by all co-authors. All authors have given approval to the final version of the manuscript.

Notes

The authors declare no competing financial interest.

ACKNOWLEDGMENTS

This work was supported by National Key Research Program (2019YFA0905800, 2018YFA0902301) and NSFC Programs (22090053, 21991080, 22074037 and 21874040).

REFERENCES

(1) Quevedo, M.; Meert, L.; Dekker, M. R.; Dekkers, D. H. W.; Brandsma, J. H.; van den Berg, D. L. C.; Ozgur, Z.; van IJcken, W. F. J.; Demmers, J.; Fornerod, M.; Poot, R. A. Mediator complex interaction partners organize the transcriptional network that defines neural stem cells. *Nat. Commun.* **2019**, *10* (1), 2669.

(2) Hu, W.; Yuan, Y.; Wang, C.; Tian, H.; Guo, A.; Nie, H.; Hu, H.; Tan, M.; Tang, Z.; Chen, X. Genetically Encoded Residue-Selective Photo-Crosslinker to Capture Protein-Protein Interactions in Living Cells. *Chem.* **2019**, *5* (11), 2955−2968.

(3) Rose, H. M.; Witte, C.; Rossella, F.; Klippel, S.; Freund, C.; Schröder, L. Development of an antibody-based, modular biosensor for 129Xe NMR molecular imaging of cells at nanomolar concentrations. *Proc. Natl. Acad. Sci. U. S. A.* **2014**, *111* (32), 11697−11702.

(4) Chen, T.; Tian, X.; Liu, C.; Ge, J.; Chu, X.; Li, Y. Fluorescence activation imaging of cytochrome c released from mitochondria using aptameric nanosensor. *J. Am. Chem. Soc.* **2015**, *137* (2), 982−989.

(5) Xie, S.; Qiu, L.; Cui, L.; Liu, H.; Sun, Y.; Liang, H.; Ding, D.; He, L.; Liu, H.; Zhang, J.; Chen, Z.; Zhang, X.; Tan, W. Reversible and Quantitative Photoregulation of Target Proteins. *Chem.* **2017**, *3* (6), 1021−1035.

(6) Della Corte, D.; van Beek, H. L.; Syberg, F.; Schallmey, M.; Tobola, F.; Cormann, K. U.; Schlicker, C.; Baumann, P. T.; Krumbach, K.; Sokolowsky, S.; Morris, C. J.; Grünberger, A.; Hofmann, E.; Schröder, G. F.; Marienhagen, J. Engineering and application of a biosensor with focused ligand specificity. *Nat. Commun.* **2020**, *11* (1), 4851.

(7) Yu, R.; Ying, Y.; Gao, R.; Long, Y. Confined nanopipette sensing: from single molecules, single nanoparticles, to single cells. *Angew. Chem., Int. Ed.* **2019**, *58* (12), 3706−3714.

(8) He, X.; Zhang, K.; Li, T.; Jiang, Y.; Yu, P.; Mao, L. Micrometer-scale ion current rectification at polyelectrolyte brush-modified micropipets. *J. Am. Chem. Soc.* **2017**, *139* (4), 1396−1399.

(9) Wang, D.; Mirkin, M. V. Electron-transfer gated ion transport in carbon nanopipets. *J. Am. Chem. Soc.* **2017**, *139* (34), 11654−11657.

(10) Lin, K.; Lin, C.; Polster, J. W.; Chen, Y.; Siwy, Z. S. Charge inversion and calcium gating in mixtures of ions in nanopores. *J. Am. Chem. Soc.* **2020**, *142* (6), 2925−2934.

(11) Zhang, X.; Oleinick, A.; Jiang, H.; Liao, Q.; Qiu, Q.; Svir, I.; Liu, Y.; Amatore, C.; Huang, W. Electrochemical Monitoring of ROS/RNS Homeostasis Within Individual Phagolysosomes Inside Single Macrophages. *Angew. Chem., Int. Ed.* **2019**, *131* (23), 7835−7838.

(12) Hu, K.; Li, Y.; Rotenberg, S. A.; Amatore, C.; Mirkin, M. V. Electrochemical Measurements of Reactive Oxygen and Nitrogen Species inside Single Phagolysosomes of Living Macrophages. *J. Am. Chem. Soc.* **2019**, *141* (11), 4564−4568.

(13) Jayant, K.; Hirtz, J. J.; Plante, I. J.-L.; Tsai, D. M.; De Boer, W. D. A. M.; Semonche, A.; Peterka, D. S.; Owen, J. S.; Sahin, O.; Shepard, K. L.; Yuste, R. Targeted intracellular voltage recordings from dendritic spines using quantum-dot-coated nanopipettes. *Nat. Nanotechnol.* **2017**, *12* (4), 335−344.

(14) Freedman, K. J.; Otto, L. M.; Ivanov, A. P.; Barik, A.; Oh, S. H.; Edel, J. B. Nanopore sensing at ultra-low concentrations using single-molecule dielectrophoretic trapping. *Nat. Commun.* **2016**, *7* (1), 10217.

(15) Chen, K.; Gularek, F.; Liu, B.; Weinhold, E.; Keyser, U. F. Electrical DNA Sequence Mapping Using Oligodeoxynucleotide Labels and Nanopores. *ACS Nano* **2021**, *15* (2), 2679−2685.

(16) Pan, R. R.; Hu, K. K.; Jia, R.; Rotenberg, S. A.; Jiang, D.; Mirkin, M. V. Resistive-pulse sensing inside single living cells. *J. Am. Chem. Soc.* **2020**, *142* (12), 5778−5784.

(17) Karnik, R.; Duan, C. H.; Castelino, K.; Daiguji, H.; Majumdar, A. Rectification of ionic current in a nanofluidic diode. *Nano Lett.* **2007**, *7* (3), 547−551.

(18) Chen, C. C.; Zhou, Y.; Baker, L. A. Single-nanopore investigations with ion conductance microscopy. *ACS Nano* **2011**, *5* (10), 8404−8411.

(19) Umehara, S.; Karhanek, M.; Davis, R. W.; Pourmand, N. Label-free biosensing with functionalized nanopipette probes. *Proc. Natl. Acad. Sci. U. S. A.* **2009**, *106* (12), 4611−4616.

(20) Nascimento, R. A.; Özel, R. E.; Mak, W. H.; Mulato, M.; Singaram, B.; Pourmand, N. Single cell "glucose nanosensor" verifies elevated glucose levels in individual cancer cells. *Nano Lett.* **2016**, *16* (2), 1194−1200.

(21) Song, J.; Xu, C.; Huang, S.; Lei, W.; Ruan, Y.; Lu, H.; Zhao, W.; Xu, J.; Chen, H. Ultrasmall nanopipette: toward continuous monitoring of redox metabolism at subcellular level. *Angew. Chem., Int. Ed.* **2018**, *57* (40), 13226−13230.

(22) Ying, Y.; Hu, Y.; Gao, R.; Yu, R.; Gu, Z.; Lee, L.; Long, Y. Asymmetric nanopore electrode-based amplification for electron transfer imaging in live cells. *J. Am. Chem. Soc.* **2018**, *140* (16), 5385−5392.

(23) Muttenthaler, M.; King, G. F.; Adams, D. J.; Alewood, P. F. Trends in peptide drug discovery. *Nat. Rev. Drug Discovery* **2021**, *20* (4), 309−325.

(24) Wu, L.; Ahmadvand, D.; Su, J.; Hall, A.; Tan, X.; Farhangrazi, Z. S.; Moghimi, S. M. Crossing the blood-brain-barrier with

nanoligand drug carriers self-assembled from a phage display peptide. *Nat. Commun.* **2019**, *10* (1), 4635.
(25) Knighton, D. R.; Zheng, J.; Ten Eyck, L. F.; Ashford, V. A.; Xuong, N.-H.; Taylor, S. S.; Sowadski, J. M. Crystal structure of the catalytic subunit of cyclic adenosine monophosphate-dependent protein kinase. *Science.* **1991**, *253* (5018), 407−414.
(26) Glass, D B; Cheng, H C; Mende-Mueller, L; Reed, J; Walsh, D A Primary structural determinants essential for potent inhibition of cAMP-dependent protein kinase by inhibitory peptides corresponding to the active portion of the heat-stable inhibitor protein. *J. Biol. Chem.* **1989**, *264* (15), 8802−8810.
(27) Kubota, K.; Anjum, R.; Yu, Y.; Kunz, R. C; Andersen, J. N; Kraus, M.; Keilhack, H.; Nagashima, K.; Krauss, S.; Paweletz, C.; Hendrickson, R. C.; Feldman, A. S.; Wu, C.; Rush, J.; Villén, J.; Gygi, S. P. Sensitive multiplexed analysis of kinase activities and activity-based kinase identification. *Nat. Biotechnol.* **2009**, *27* (10), 933−940.
(28) Xu, Y. H.; Shi, W.; He, X. Y.; Wu, X. F.; Li, X. H.; Ma, H. M. Facile and sensitive method for protein kinase A activity assay based on fluorescent off-on polyU-peptide assembly. *Anal. Chem.* **2017**, *89* (20), 10980−10984.
(29) Cadinu, P.; Campolo, G.; Pud, S.; Yang, W.; Edel, J. B.; Dekker, C.; Ivanov, A. P. Double barrel nanopores as a new tool for controlling single-molecule transport. *Nano Lett.* **2018**, *18* (4), 2738−2745.
(30) Kubeil, C.; Bund, A. The Role of Nanopore Geometry for the Rectification of Ionic Currents. *J. Phys. Chem. C* **2011**, *115* (16), 7866−7873.
(31) Panday, N.; Qian, G.; Wang, X.; Chang, S.; Pandey, P.; He, J. Simultaneous ionic current and potential detection of nanoparticles by a multifunctional nanopipette. *ACS Nano* **2016**, *10* (12), 11237−11248.
(32) Calander, N. Analyte Concentration at the Tip of a Nanopipette. *Anal. Chem.* **2009**, *81* (20), 8347−8353.
(33) Siwy, Z.; Heins, E.; Harrell, C. C.; Kohli, P.; Martin, C. R. Conical nanotube ion current rectifiers: the role of surface charge. *J. Am. Chem. Soc.* **2004**, *126* (35), 10850−1085.
(34) Mu, C. J.; LaVan, D. A.; Langer, R. S.; Zetter, B. R. Self-assembled gold nanoparticle molecular probes for detecting proteolytic activity in vivo. *ACS Nano* **2010**, *4* (3), 1511−1520.
(35) Borle, A. B. Kinetic analyses of calcium movements in HeLa cell cultures. *J. Gen Physiol.* **1969**, *53* (1), 43−56.
(36) Zhang, Q.; Huang, H.; Zhang, L.; Wu, R.; Chung, C.; Zhang, S.; Torra, J.; Schepis, A.; Coughlin, S. R.; Kornberg, T. B.; Shu, X. Visualizing dynamics of cell signaling in vivo with a phase separation-based kinase reporter. *Mol. Cell* **2018**, *69* (2), 334−346.
(37) Vilozny, B.; Actis, P.; Seger, R. A.; Vallmajo-Martin, Q.; Pourmand, N. Reversible cation response with a protein-modified nanopipette. *Anal. Chem.* **2011**, *83* (16), 6121−6126.
(38) Zhang, X.; Candas, M.; Griko, N. B.; Taussig, R.; Bulla, L. A mechanism of cell death involving an adenylyl cyclase/PKA signaling pathway is induced by the Cry1Ab toxin of Bacillus thuringiensis. *Proc. Natl. Acad. Sci. U. S. A.* **2006**, *103* (26), 9897−9902.
(39) Zhang, J.; Ma, Y. L.; Taylor, S. S.; Tsien, R. Y. Genetically encoded reporters of protein kinase A activity reveal impact of substrate tethering. *Proc. Natl. Acad. Sci. U. S. A.* **2001**, *98* (26), 14997−15002.
(40) Allen, M.; DiPilato, L. M.; Rahdar, M.; Ren, Y.; Chong, C.; Liu, J.; Zhang, J. Reading dynamic kinase activity in living cells for high-throughput screening. *ACS Chem. Biol.* **2006**, *1* (6), 371−376.

https://doi.org/10.1021/acsnano.1c10796
ACS Nano 2022, 16, 5752−5763